Resonant pseudo-Dirac dark matter as a sub-GeV thermal target

Nirmalya Brahma, Saniya Heeba, and Katelin Schutz
Department of Physics and Trottier Space Institute, McGill University, Montréal, QC H3A 2T8, Canada

(Received 11 August 2023; accepted 2 January 2024; published 8 February 2024)

Dark matter (DM) could be a pseudo-Dirac thermal relic with a small mass splitting that is coupled off diagonally to a kinetically mixed dark photon. This model, particularly in the sub-GeV mass range, is a key benchmark for accelerator searches and direct detection experiments. Typically, the presence of even a tiny fraction of pseudo-Dirac DM in the excited state around the time of recombination would be excluded by DM annihilation bounds from the cosmic microwave background (CMB); thus, viable thermal histories must typically feature an exponential suppression of the excited state. We revisit assumptions about the thermal history in the resonant regime, where the dark photon mass is slightly more than twice the DM mass (to within ∼10%), leading to an s-channel resonance in the annihilation cross section. This resonance substantially reduces the couplings required for achieving the observed relic abundance, implying that in much of the parameter space, the DM kinetically decouples from the Standard Model well before the final DM relic abundance is achieved. We find that the excited state is not thermally depopulated in this regime. In spite of this, we find that the presence of the excited state does *not* violate CMB bounds, even for arbitrarily small mass splittings. The present-day abundance of the excited state opens up the possibility of signatures that are usually not relevant for pseudo-Dirac DM, including indirect detection, direct detection, and self-interacting DM signatures.

DOI: 10.1103/PhysRevD.109.035006

I. INTRODUCTION

The origin of dark matter (DM) remains an elusive mystery. If the DM thermalizes with the Standard Model (SM) plasma in the early Universe, then thermal freeze-out provides a compelling explanation for the observed abundance of DM. In particular, thermal freeze-out is relatively insensitive to the initial conditions of the early Universe, and the relevant couplings can be probed in a number of ways using direct detection, indirect detection, and collider observables [1]. If the DM is lighter than the ∼GeV scale, then the Lee-Weinberg bound [2] implies that the mediator for DM-SM interactions cannot be a SM force carrier, which opens up the possibility of a "dark sector," with auxiliary forces and matter fields beyond just DM. A simple, technically natural example of a new mediator is a dark photon that kinetically mixes with the SM photon [3–12]. Given the null detection of weak-scale DM thus far (see, e.g., Refs. [13,14]), lighter dark sectors are of increasing interest to the community (see, e.g., Refs. [15–19]), and there is a range of new and proposed experimental methodologies that will be sensitive to these DM candidates [20–26].

The standard thermal freeze-out mechanism for sub-GeV DM is subject to strong bounds from cosmic microwave background (CMB) anisotropies assuming annihilation through an s-wave process to visible SM particles. Even after freeze-out, DM can still annihilate at a sub-Hubble rate and inject considerable energy into the SM plasma near the time of recombination. Energy injection in the form of visible particles would observably modify the properties of the plasma even if the DM annihilations are extremely rare, since a ∼part-per-billion fraction of the DM annihilating would be enough energy injection to ionize all the atoms in the Universe. Considering the effects on CMB anisotropies as measured by *Planck*, current bounds on DM annihilation rule out s-wave thermal freeze-out of DM below ∼10 GeV, with the exact value depending on the SM final state [27,28].

A well-studied way to bring s-wave freeze-out into consistency with CMB constraints is by introducing a small mass splitting between nondegenerate DM states [29–35]. There is no symmetry that prevents Dirac fermions from splitting into two Majorana mass states, and this is easily realized in models where DM is charged under some new dark gauge symmetry at high energies which is broken at low energies [36,37]. The dark matter multiplet, consisting of χ_1 and χ_2, acquires a mass splitting $\delta = m_{\chi_2} - m_{\chi_1}$, which can be naturally small if the dark symmetry is approximate (for example, the small neutron-proton mass splitting is protected by an approximate isospin symmetry). In this work, we do not specify the origin of the mass splitting and

treat it phenomenologically. However, we note that small mass splittings are generally easy to accommodate from a model-building perspective in situations with a small overall mass scale and small couplings [29,38–41]. In this model, the couplings of DM with the dark photon are purely off diagonal, i.e., the only vertex with the dark photon couples χ_1 and χ_2. For this reason, annihilation rates to SM final states can be significantly reduced because the leading-order tree-level annihilation process requires a large χ_2 abundance, which may be thermally depleted like $e^{-\delta/T}$ at temperatures $T \lesssim \delta$ [41,42]. Given the ∼eV-scale temperatures that are relevant for recombination, mass splittings with $\delta \gtrsim 1$ eV can be compatible with CMB constraints in parts of the parameter space (with larger mass splittings being unconstrained for a wider range of couplings and DM masses).

Alternatively, if the DM annihilation occurs close to a pole in the cross section (for instance when the mediator is close to twice the DM mass), then the relevant couplings to achieve the observed relic abundance can be lowered substantially [43,44]. If this pole is relevant for setting the DM abundance at early times but not during the recombination epoch, then the CMB bounds are relaxed because of the lower off resonance annihilation rate to SM final states. The CMB bounds were carefully studied in Ref. [45] for the case of Dirac DM interacting with a dark photon with $m_{A'} \approx 2m_\chi$. Meanwhile, the resonant regime for inelastic pseudo-Dirac DM has been studied primarily in the context of its signature at colliders given the modification to the predicted couplings [38,46–48]. The cosmology of resonant pseudo-Dirac DM, on the other hand, has yet to be studied in detail. In particular, the substantial effects of early kinetic decoupling of the DM have been overlooked so far.

In this work, we perform a comprehensive study of the cosmology of pseudo-Dirac DM in the resonant regime. We find that even in the mildly resonant regime with $(m_{A'} - 2m_\chi)/m_{A'} \sim 10\%$, pseudo-Dirac DM can have arbitrarily low mass splittings without violating limits from the CMB. Moreover, we find that in most of the parameter space the excited state has a high relic fraction. This provides a strong contrast to most pseudo-Dirac thermal histories which feature an exponential suppression of the excited state due to thermal depletion. Accordingly, the cosmology and astrophysics of this DM candidate are quite different from the usual pseudo-Dirac parameter space, as are the direct and indirect DM detection signatures.

The rest of this article is organized as follows. In Sec. II, we review the model and the relevant processes that affect the cosmology of this DM candidate in the early Universe. In particular, we solve the Boltzmann equations for the density and temperature evolution of the DM states χ_1 and χ_2. In Sec. III, we consider cosmological and astrophysical signatures including big bang nucleosynthesis, the CMB, self-interacting DM (SIDM), and indirect detection. In Sec. IV we discuss prospects for detecting this DM candidate using terrestrial experimental methods. Discussion and concluding remarks follow in Sec. V.

II. EARLY UNIVERSE BEHAVIOR

A. Pseudo-Dirac DM parameter space

We consider a light ($m_\chi \lesssim 10$ GeV) pseudo-Dirac DM model with its relic abundance set by annihilation to SM final states via a dark photon mediator. We focus on this mass range primarily because Dirac DM with $m_\chi \lesssim 10$ GeV is excluded by the CMB for s-wave freeze-out to visible final states [28]. In this model, the interaction terms are

$$\mathcal{L} \supset \frac{\kappa}{2} F'_{\mu\nu} F^{\mu\nu} + i g_\chi A'_\mu \chi_2 \gamma^\mu \chi_1, \tag{1}$$

where $\chi_{2,1}$ are the excited and ground states, respectively, that couple with interaction strength g_χ to a vector mediator A' that kinetically mixes with the SM photon with mixing parameter κ. We focus on parameter space where the mass splitting is much smaller than the DM mass, $\delta = m_{\chi_2} - m_{\chi_1} \ll m_{\chi_1}$. In the following discussion, we denote the average mass of the two states as m_χ. We are furthermore interested in the resonant regime where $m_{A'} \approx m_{\chi_2} + m_{\chi_1} = 2m_{\chi_1} + \delta = 2m_\chi$. We parametrize the proximity to resonance with the parameter

$$\epsilon_R = \frac{m_{A'}^2 - s_0}{s_0}, \tag{2}$$

where $s_0 = (m_{\chi_1} + m_{\chi_2})^2$. In this work, we consider $\epsilon_R \in [0.001, 0.1]$. The lower limit is motivated by photodisassociation bounds coming from big bang nucleosynthesis (BBN) as discussed in Sec. III A. On the other hand, as $\epsilon_R > 0.1$, we approach the nonresonant limit. We remain agnostic about the mechanism responsible for generating the mass splitting as well as the resonance; however the parameters we consider are self-consistent even in a minimal UV setup. For instance, we could consider a complex dark Higgs with a dark charge of 2 interacting with a Dirac fermion with a mass m_D [36,37,49]. The breaking of the dark $U(1)$ symmetry through the vacuum expectation value of the dark Higgs, v_D, then results in both the mass term for the dark photon as well as a Majorana mass term for the Dirac fermion which generates the mass splitting. If the dark Higgs is heavy with $v_D \gg m_D$ then it will not participate in the dynamics that determine the DM thermal history. With this hierarchy in mind, having the dark photon mass near its resonant value pushes $g_\chi \sim m_D/v_D \ll 1$, which we show below is consistent with setting the observed DM relic abundance in the resonant regime. Finally, the mass splitting is determined by the Yukawa coupling of the Dirac fermion y_χ, with $\delta \sim y_\chi v_D$.

Though the dark photon is the mediator of this model, it can be resonantly produced on shell via inverse decays. The dark photon can subsequently decay invisibly,

$$\Gamma_{\rm DM} = \frac{g_\chi^2 m_{A'}}{12\pi}\sqrt{1-\frac{s_0}{m_{A'}^2}}\left(1+\frac{s_0}{2m_{A'}^2}\right)\left(1-\frac{\delta^2}{m_{A'}^2}\right)^{3/2}, \quad (3)$$

or visibly to SM final states,

$$\Gamma_{\rm SM} = R(m_{A'})\Gamma_{\mu^+\mu^-} + \sum_\ell \Gamma_{\ell^+\ell^-}, \quad (4)$$

where $R(m_{A'})$ is the empirically determined branching ratio of $\sigma(e^+e^- \to \text{hadrons})/\sigma(e^+e^- \to \mu^+\mu^-)$ [50,51] at center-of-mass energy $\sqrt{s} = m_{A'}$ and

$$\Gamma_{\ell^+\ell^-} = \frac{\kappa^2 e^2 m_{A'}}{12\pi}\sqrt{1-\frac{4m_\ell^2}{m_{A'}^2}}\left(1+\frac{2m_\ell}{m_{A'}}\right). \quad (5)$$

The total on shell decay width is $\Gamma_{A'} \equiv \Gamma_{\rm DM} + \Gamma_{\rm SM} \equiv \Gamma_{\rm DM} + \Gamma_{e^+e^-}/B_e$, where B_e is the branching ratio of the dark photon to electrons.

B. Relic density assuming thermal equilibrium

In our parameter region of interest, DM obtains its relic abundance when s-channel processes like $\chi_1\chi_2 \to \text{SM SM}$ become inactive, usually well after chemical freeze-out for $\epsilon_R \ll 1$. Using the formalism developed in Ref. [47], the corresponding thermally averaged cross section can be written as

$$\langle\sigma v\rangle = \frac{2x}{K_2^2(x)}\int_0^\infty d\epsilon\, \sigma v\sqrt{\epsilon}(1+2\epsilon)K_1\left(2x\sqrt{1+\epsilon}\right), \quad (6)$$

where $x = m_{\chi_1}/T$, $\epsilon = (s-s_0)/s_0$ is a dimensionless measure of the kinetic energy and

$$\sigma v = F(\epsilon)\frac{m_{A'}\Gamma_{A'}}{(s-m_{A'}^2)^2 + m_{A'}^2\Gamma_{A'}^2} \quad (7)$$

with

$$F(\epsilon) = \frac{4\pi\kappa^2\alpha\alpha_D}{3s_0 m_{A'}\Gamma_{A'}}\frac{(3+2\epsilon)[(1+\epsilon)s_0+2m_e^2]}{(1+\epsilon)(1+2\epsilon)B_e(\sqrt{s_0(1+\epsilon)})} \times [s_0(1+\epsilon)-4m_e^2]^{1/2}[s_0(1+\epsilon)-\delta^2]^{1/2}. \quad (8)$$

The thermally averaged cross section can be further reduced to semianalytic forms in the nonrelativistic ($\epsilon \ll 1$) and resonant ($\epsilon \approx \epsilon_R$) limits [45].

In order to calculate the *total* DM relic density, one needs to solve the Boltzmann equation for $\chi_1\chi_2 \to \text{SM SM}$,

$$\frac{dY_{\rm tot}}{dx} = \frac{s}{Hx}\langle\sigma v\rangle_{\rm eff}(Y_{\rm tot}^2 - Y_{\rm tot,eq}^2), \quad (9)$$

where $Y_{\rm tot} = Y_{\chi_1} + Y_{\chi_2}$ is the total comoving density for DM with $Y_{\chi_1,\chi_2} = n_{\chi_1,\chi_2}/s$, s is the entropy density, and the effective thermally averaged cross section is [43,47]

$$\langle\sigma v\rangle_{\rm eff} = \frac{2(1+\delta/m_\chi)^{3/2}e^{-x\delta/m_{\chi_1}}}{(1+(1+\delta/m_{\chi_1})^{3/2}e^{-x\delta/m_{\chi_1}})^2}\langle\sigma v\rangle. \quad (10)$$

The total DM relic density is then given by

$$\Omega_{\rm DM}h^2 = 8.77\times10^{-11}\left[\int_{x_f}^\infty dx\frac{\langle\sigma v\rangle_{\rm eff}}{x^2}g_*^{1/2}\right]^{-1}, \quad (11)$$

where g_* correspond to the effective relativistic degrees of freedom in the early Universe. It can be seen from Eqs. (6) and (7) that the cross section is resonantly enhanced when χ_1 and χ_2 have enough energy to produce the A' on shell, leading to very efficient annihilation at a temperature $T \sim \epsilon_R m_{\chi_1}$. Owing to the resonant enhancement, as $\epsilon_R \to 0$ even very tiny couplings are able to efficiently deplete the DM in the early Universe to obtain the observed DM relic density.

C. Early kinetic decoupling

A crucial caveat to the relic density calculation detailed above is that it assumes that the DM and SM remain in kinetic equilibrium while annihilations are active (including after chemical freeze-out) through scattering processes, primarily off of electrons $\chi_1 e \leftrightarrow \chi_2 e$. Since this is a t-channel process, it does not benefit from the same resonant enhancement as the s-channel annihilations. Therefore, when the couplings between the two sectors are small, the assumption of kinetic equilibrium may no longer hold, and DM can kinetically decouple well before DM annihilation $\chi_1\chi_2 \to \text{SM SM}$ hits its resonance (compare, e.g., the dashed and solid lines in Fig. 1). In fact, as shown in Fig. 1, scattering processes decouple before annihilation in much of the parameter space. As a result, to accurately calculate the DM relic density, one needs to solve a coupled system of differential equations tracking the evolution of both the DM number density as well as the dark sector temperature, $y(x) \equiv m_{\chi_1}T_{\rm DM}s^{-2/3}$ [52–54],

$$\frac{Y'}{Y} = \frac{sY}{x\tilde{H}}\left(\frac{Y_{\rm eq}^2}{Y^2}\langle\sigma v\rangle - \langle\sigma v\rangle_{\rm neq}\right) \quad (12)$$

$$\frac{y'}{y} = \frac{\gamma(T)}{x\tilde{H}}\left(\frac{y_{\rm eq}}{y}-1\right) + \frac{sY}{x\tilde{H}}(\langle\sigma v\rangle_{\rm neq} - \langle\sigma v\rangle_{2,\rm neq}) + \frac{sY}{x\tilde{H}}\frac{Y_{\rm eq}^2}{Y^2}\left[\frac{y_{\rm eq}}{y}\langle\sigma v\rangle_2 - \langle\sigma v\rangle\right] + \frac{H}{x\tilde{H}}\frac{\langle p^4/E^3\rangle_{\rm neq}}{3T_{\rm DM}}, \quad (13)$$

where $\tilde{H}$ is the normalized Hubble rate as defined in Ref. [53] and the subscript "neq" denotes that the corresponding thermal average is over the DM phase distribution at a temperature $T_{\rm DM}$ distinct from the SM temperature T, i.e., assuming DM is not necessarily in kinetic equilibrium with the SM. Additionally, $\langle\sigma v\rangle_2$ is a temperature-weighted analog of the usual thermally averaged annihilation cross section $\langle\sigma v\rangle$, as defined in Ref. [53], and $\gamma(T)$ is the

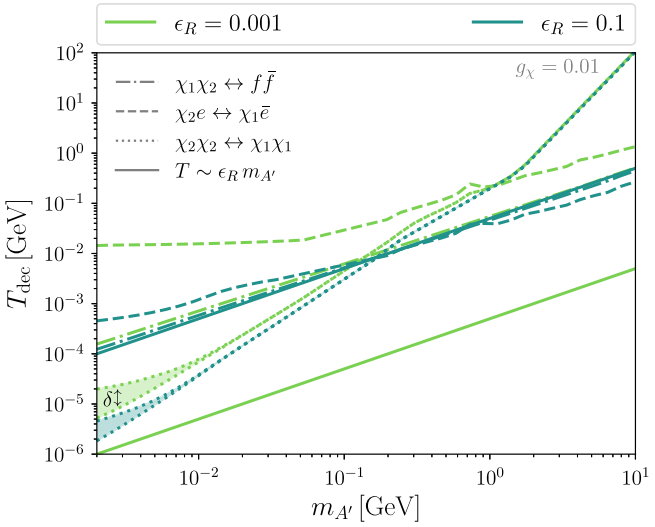

FIG. 1. The SM temperature as a function of the dark photon mass at which DM-SM scattering (dashed), DM-DM scattering (dotted), and DM-DM annihilation (dot-dashed) decouple for $\epsilon_R = 0.001$ (light green) and $\epsilon_R = 0.1$ (dark green), with $g_\chi = 0.01$. The solid lines show when annihilation becomes resonant, with $T \sim \epsilon_R m_{A'}$. For each parameter point in this plot κ is chosen so as to obtain the observed DM relic abundance ignoring the effects of early kinetic decoupling. The shaded areas between dotted lines correspond to varying δ between 1 and 100 eV, from bottom to top. In some parts of the parameter space, resonant depletion of the DM abundance occurs much later than other decoupling processes, indicating that the early decoupling can influence the subsequent relic DM abundance.

DM-SM momentum transfer rate which is a measure of DM-SM elastic scattering. Terms involving scattering and annihilation can both keep the DM temperature coupled to the SM. These Boltzmann equations have been extensively studied for the case of elastically decoupling relics [52–55]. For inelastic DM models, the corresponding Boltzmann equations may have an additional dependence on the mass splitting δ, which would appear in various cross sections, and there could also in principle be separate thermal evolution of the ground and excited state species. However, in our parameter region of interest, $\delta \ll m_\chi$ and δ is also much smaller than the decoupling temperatures for all relevant processes. Therefore, we explicitly find that the thermal history of this model behaves, to a very good approximation, as a strictly Dirac model during the temperatures relevant for freeze-out. Therefore, to calculate the relic pseudo-Dirac DM density, we use the publicly available Boltzmann solver DRAKE [54] modified for a resonant Dirac DM model.

D. Parameter space

The couplings required to reproduce the observed DM abundance are shown in Fig. 2 for different values of m_χ and ϵ_R. Note that δ is generally much smaller than all the temperatures that are relevant for setting the relic abundance, and therefore it is irrelevant in determining the couplings. As expected, for a given DM mass, smaller values of ϵ_R (indicated by thinner lines) result in a larger resonant enhancement in the annihilation cross section, and correspond to smaller couplings reproducing the relic density, thereby shifting the lines downward and to the left. For a fixed value of m_χ and ϵ_R, the shape of the curve in the g_χ-κ plane can be explained by considering the thermally averaged cross section in the limit $\epsilon_R \ll 1$. In this case, as was pointed out in Ref. [45], the slower decay ($\Gamma_{\rm SM}$ vs $\Gamma_{\rm DM}$) is the bottleneck in terms of determining the final DM abundance,

$$\Omega_{\rm DM} h^2 \propto \frac{\Gamma_{A'}}{\kappa^2 g_\chi^2}. \tag{14}$$

This implies that for $g_\chi \ll \kappa$ ($\kappa \ll g_\chi$), the relic density becomes independent of κ (g_χ) resulting in the asymptotic behavior seen in Fig. 2.

In the limit $\epsilon_R \to 0$, we find that the relic density obtained using the coupled system of Boltzmann Eqs. (12) and (13) differs from the standard Boltzmann treatment (i.e., assuming identical SM and DM temperatures) by at most a factor of ∼2. For $\epsilon_R \sim 1$, one would naively expect the difference to be even smaller since we are not only further off resonance but are also pushed toward larger couplings where the expectation is that kinetic equilibrium should be maintained more easily. However, we find that the difference between the two treatments can be as large as an order of magnitude in the relic density in the region $\epsilon_R \sim 0.1$. This can be attributed to the deviation of the DM temperature from the SM temperature and was earlier discussed in the context of scalar singlet DM in Ref. [56]. In particular, for $\epsilon_R \ll 0.1$, the deviation is very small and positive, $T_{\rm DM} \gtrsim T$ whereas for $\epsilon_R \sim 0.1$ the deviation is large and negative, $T_{\rm DM} \ll T$ (see also the bottom panel of Fig. 3). Although one can numerically estimate the sign and magnitude of this deviation by studying the interplay of the various terms on the right-hand side of Eq. (13), they can also be understood qualitatively by considering the underlying DM phase space during and after chemical freeze-out.

Under the assumption that DM has already kinetically decoupled, the final DM density can be assumed to be proportional to the annihilation cross section averaged over the DM temperature, $\langle \sigma v \rangle_{\rm neq}$ [in analogy with Eq. (11)]

$$\Omega_{\rm DM} h^2 \propto \left[\int_{x_f}^{\infty} {\rm d}x \frac{\langle \sigma v \rangle_{\rm neq}}{x^2} \right]^{-1}. \tag{15}$$

In general, as $\epsilon_R \to 0$, the DM particles need only very little momentum to hit the resonance and annihilate efficiently, implying that resonant annihilation depletes the low-momentum tail of the DM distribution and shifts the average DM momentum (and therefore the temperature)

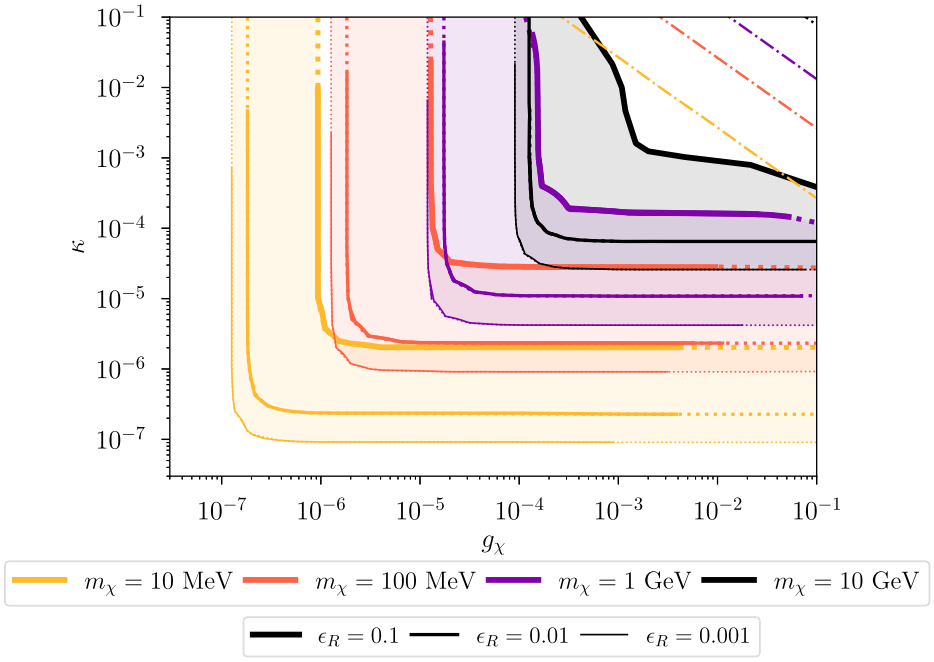

FIG. 2. The couplings that yield a DM abundance that matches the observed relic density for various DM masses and values of ϵ_R. Dashed lines indicate CMB annihilation constraints on those couplings, while solid lines are consistent with the CMB. In this parameter space, the smaller of the two couplings (corresponding to whichever decay channel is the bottleneck) determines the relic abundance, with the larger coupling being irrelevant. Small deviations from this behavior occur at large values of m_χ and ϵ_R where early kinetic decoupling has a significant effect on the relic abundance. These trends contrast with the parameter space for standard thermal freeze-out where the product of couplings is the most relevant for setting the relic abundance. For comparison, we show the couplings for thermal freeze-out for $m_{A'} = 3m_\chi$ (off resonance) as dot-dashed lines.

to larger values. During chemical freeze-out, since the average DM momentum is already large, only a small fraction of DM particles can annihilate resonantly. The increase in the DM temperature further decreases the available phase space for resonant annihilation and therefore decreases $\langle\sigma v\rangle_{\rm neq}$. This results in the small dip in $\langle\sigma v\rangle_{\rm neq}$ for $\epsilon_R = 0.001$ around chemical freeze-out $x_f \sim 20$ seen in the top panel of Fig. 3 and corresponds to reducing the efficiency of DM annihilations and increasing its abundance. After DM has chemically decoupled, its temperature now redshifts as matter, and therefore DM cools much faster than the SM, increasing the relative number of DM particles with low momentum. As a result, resonant annihilation which is active at $T_{\rm DM} \sim \epsilon_R m_\chi$ happens at slightly earlier times (since $T_{\rm DM} \ll T$) compared to the kinetically coupled case when they occur at $T \sim \epsilon_R m_\chi$. Hence, resonant annihilation is more efficient in depleting the DM [due to the x dependence of Eq. (15)]. Since these two effects change the relic density in opposing ways, the final relic density is only slightly different from the kinetically coupled case. This is especially true given that the $1/x^2$ weighting in the integral of Eq. (15) ensures that the most substantial contributions to the relic abundance come from early times before the difference between $\langle\sigma v\rangle_{\rm eq}$ and $\langle\sigma v\rangle_{\rm neq}$ becomes too large.

For $\epsilon_R \sim 0.1$, on the other hand, DM particles need larger momentum to annihilate resonantly, and therefore resonant annihilations shift the average DM momentum (and temperature) to smaller values. Additionally, resonant annihilation is active exactly during chemical freeze-out, $x_{\rm DM} \sim \epsilon_R^{-1} \sim x_f$. This implies that if DM is kinetically decoupled, the depletion in the large-momentum DM phase space effectively turns off resonant annihilations quite quickly as shown by the dark green line in the top panel of Fig. 3. Furthermore, the x^2 scaling of Eq. (15) in this regime enhances the difference in the total relic abundance since $\langle\sigma v\rangle_{\rm eq}$ and $\langle\sigma v\rangle_{\rm neq}$ differ substantially around the time of chemical freeze-out. As a result, the relic density is significantly altered: DM is overproduced, and larger couplings are required to obtain the observed DM abundance.

E. Late-time abundance of the excited state

The relative fraction of excited-state particles, $f^* = n_{\chi_2}/n_{\chi_1}$ is a key quantity in determining the impact of late-time DM behavior in cosmological environments as well as terrestrial experiments, as discussed further in Secs. III and IV. Even if DM is symmetrically produced in the ground and excited states, the ground and excited states can interconvert through processes within the dark sector or through scattering processes with the SM as long

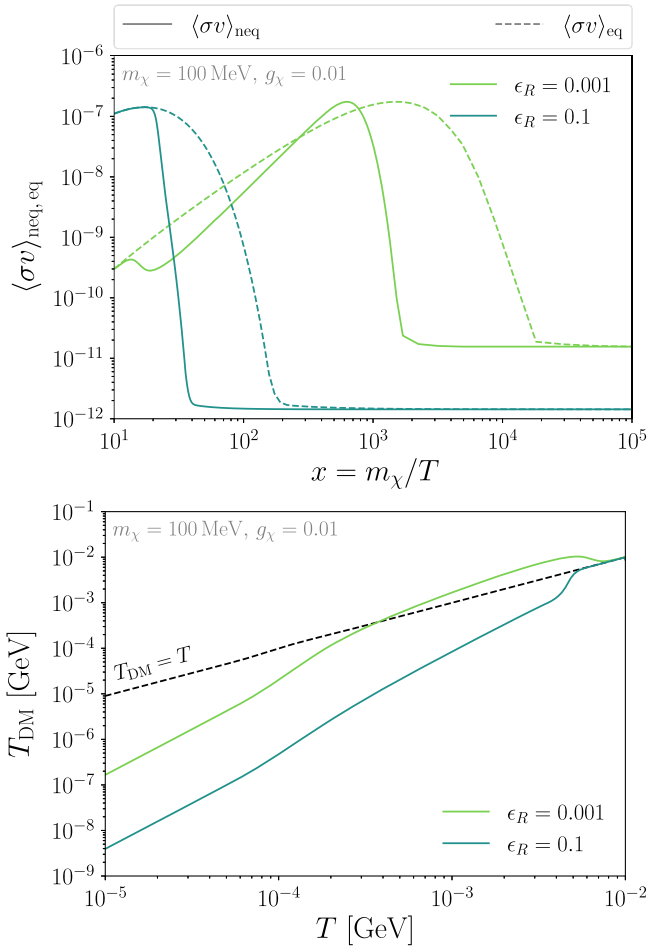

FIG. 3. Top: the thermally averaged annihilation cross section for kinetically decoupled (solid) and kinetically coupled (dashed) DM as a function of x (defined with respect to the SM temperature, T) for $\epsilon_R = 0.1$ (dark green) and $\epsilon_R = 0.001$ (light green). Early kinetic decoupling can suppress or enhance resonant annihilation at a given temperature. Bottom: the DM temperature vs the SM temperature for the same two values of ϵ_R. The black dashed line corresponds to kinetic equilibrium. Early kinetic decoupling may increase or decrease the DM temperature relative to the SM. In both panels, we fix $m_\chi = 100$ MeV, $g_\chi = 0.01$ and choose κ such that we reproduce the observed DM abundance after solving Eqs. (12) and (13).

as their rates exceed the Hubble expansion rate. In particular, as long as chemical equilibrium is maintained *within* the dark sector, the excited state number density is given by $n_{\chi_2} \sim n_{\chi_1} e^{-\delta/T_{\rm DM}}$. Chemical equilibrium in the dark sector can be maintained through DM-SM scattering, which also maintains kinetic equilibrium with the SM, $\chi_1 e \leftrightarrow \chi_2 e$, or through DM up/down-scattering, $\chi_1\chi_1 \leftrightarrow \chi_2\chi_2$. The fractional abundance of a cosmologically stable excited state at late times is determined by the DM temperature when it chemically decouples, $f^* = n_{\chi_2}/n_{\chi_1} \approx e^{-\delta/T_{\rm chem}}$, where $T_{\rm chem}$ is determined by whichever of the processes listed above decouples last, $T_{\rm chem} = \min[T_{\chi e}, T_{\chi\chi}]$, where

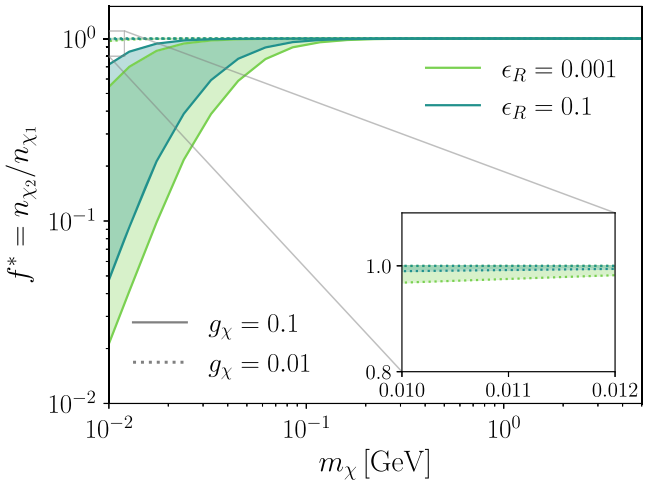

FIG. 4. The relative number density of the excited and ground states, $f^* = n_{\chi_2}/n_{\chi_1}$, as a function of the DM mass. The different lines correspond to $g_\chi = 0.1$ (solid) and $g_\chi = 0.01$ (dotted). The two colors correspond to two different values of ϵ_R, and the shaded areas correspond to varying δ between 1 and 100 eV from top to bottom. Owing to the early decoupling of the processes that would deplete the excited state, the excited state remains abundant at late times in most of the parameter space, in contrast to most other pseudo-Dirac DM thermal histories.

$$\left.\frac{n_e\langle\sigma v\rangle_{\chi_2 e\to\chi_1\bar{e}}}{H}\right|_{T=T_{\chi e}} \sim 1, \tag{16}$$

$$\left.\frac{n_{\chi_2}\langle\sigma v\rangle_{\chi_2\chi_2\to\chi_1\chi_1}}{H}\right|_{T=T_{\chi\chi}} \sim 1. \tag{17}$$

Here, n_e is the electron number density, $n_{\chi_2} = n_{\chi_1} e^{-\delta/T_{\rm DM}}$ is obtained by scaling back the present-day DM abundance $n_{\chi_1} \sim T_{\rm eq} T^3/m_{\chi_1}$, and the relevant cross sections are from Ref. [41]. If $\chi_2\chi_2 \leftrightarrow \chi_1\chi_1$ decouples after $\chi_2 e \leftrightarrow \chi_1 e$, two temperature scales enter in Eq. (17), the SM temperature T that largely determines the Hubble rate, and the DM temperature which is a function of the temperature at which DM decouples from the SM, $T_{\rm DM} \sim T^2/T_{\chi e}$.

In the standard thermal history for inelastic DM, one finds that $T_{\rm chem} \lesssim \delta$ owing to the large DM-DM and/or DM-SM couplings which ensures chemical equilibrium in the dark sector is maintained until late times. This results in a strong suppression of the excited state at late times, $f^* \sim \mathcal{O}(10^{-4})$ [42,57]. However, the small couplings present in our parameter space result in $T_{\rm chem} \gg \delta$, and therefore a similar abundance of the ground and excited state, $f^* \sim 1$ in much of the parameter space. This is represented in Fig. 4, in which we show the relative abundance of the ground and excited states as a function of the DM mass for different values of ϵ_R and g_χ. Note that $f^* \sim 1$ for $g_\chi \ll 0.1$ for all DM masses of interest. For $g_\chi \sim 0.1$, we find a suppression of the excited state to $f^* \sim 0.01$ when $m_\chi \lesssim 100$ MeV.

III. COSMOLOGICAL AND ASTROPHYSICAL CONSTRAINTS

Owing to the high late-time abundance of the excited state, this thermal history has unique signatures compared to other pseudo-Dirac DM thermal histories. In this section, we determine the qualitatively new behavior in astrophysical systems caused by the presence of the excited state and estimate the resulting constraints on the model as inferred from existing measurements.

A. BBN

Sub-GeV DM may significantly impact the abundance of light elements in the Universe produced during BBN. If DM has a thermal abundance and is relativistic at a SM temperature of a few MeV, it contributes to the number of relativistic degrees of freedom in the early Universe modifying $N_{\rm eff}$ and changing the abundances of light elements like helium. Measurements of the helium fraction can thus be used to place a lower bound on the mass of thermal DM, $m_\chi \gtrsim 10$ MeV [58,59]. In this work, we conservatively consider DM above this scale to ensure that the parameter space is not ruled out. However, we note that this constraint could be slightly weaker in parts of our parameter space due to the early kinetic decoupling of DM from the SM. In particular, if the DM decouples early enough, then some of the SM degrees of freedom in the bath at that time, given by $g_{*,0}$ in total, heat the SM bath at later times and raise the SM temperature relative to $T_{\rm DM}$ by a factor of a few in order to conserve entropy, $T_{\rm SM}/T_{\rm DM} \sim (g_{*,0}/g_{*,\rm BBN})^{1/3}$. This means that the DM contribution to the energy density, and hence $N_{\rm eff}$, could be diluted by a factor of $(g_{*,0}/g_{*,\rm BBN})^{4/3}$. Furthermore, once the DM becomes nonrelativistic at a temperature $T_{\rm DM} \sim m_\chi$, the DM temperature will drop even further relative to the SM temperature, $T_{\rm DM} \sim T_{\rm SM}^2 (g_{*,0}/g_{*,\rm BBN})^{-2/3}/m_\chi$ for $T_{\rm SM} < m_\chi$. Therefore, by the time of BBN, MeV-scale DM may have had its energy density diluted and may be nonrelativistic, thus not contributing substantially to $N_{\rm eff}$. In concert, these effects could increase the range of allowed masses for this model; we leave a more detailed exploration to future work.

In addition to the modification of $N_{\rm eff}$, DM annihilating into SM states at a temperature of a few keV can inject energy into the SM plasma causing the photodisassociation of light nuclei like deuterium. The corresponding bound on the annihilation cross section not only depends on the DM mass and the relevant final states but also depends on the temperature of the kinetic decoupling, $T_{\rm kd}$, in the case when the thermally averaged cross section has a temperature dependence [58]. In our model, the cross sections show this dependence around the keV-scale temperatures relevant for photodisassociation for $\epsilon_R \ll 1$. Accurately evaluating this bound for such small ϵ_R's is therefore nontrivial, and we leave a detailed study for future work. For the purposes of this work, we note that for a velocity-independent annihilation cross section, the bound from photo disassociation corresponds to $\sigma v \lesssim$ few $\times 10^{-25}$ cm^3/s, and the constraint for velocity dependent cross section gets weaker with increasing $T_{\rm kd}$ [58]. For resonant annihilations, even the small couplings considered in this work can result in significantly larger cross sections at the late times relevant to BBN. Since the resonant annihilation cross section peaks near $T \sim \epsilon_R m_\chi$, in this work we consider $\epsilon_R \geq 0.001$, which along with the conservative lower bound on m_χ discussed above, ensures that the DM annihilation cross section is always below the upper bound during temperatures relevant for photodisassociation.

B. Cosmic microwave background

DM annihilation into SM final states during recombination can inject energy into the SM plasma. This energy injection can alter the ionization history and affect CMB anisotropies due to the scattering of CMB photons on additional free electrons that would have otherwise recombined into neutral atoms in the standard cosmology. This injection is usually described in terms of an effective parameter [28],

$$p_{\rm ann} = 2 f^* f_{\rm eff} \frac{\langle \sigma v \rangle_{\rm CMB}}{m_\chi} < 3.2 \times 10^{-28}\ {\rm cm^3\ s^{-1}\ GeV^{-1}}, \tag{18}$$

where f^* is the fraction of DM in the excited state as described in the previous section, $f_{\rm eff}$ is the efficiency fraction of injected energy that gets deposited in the plasma (where we adopt the values from Ref. [45] using the spectra from Refs. [60,61] and which depend on the DM mass and SM final state), and $\langle \sigma v \rangle_{\rm CMB}$ is the total annihilation cross section into SM states at recombination. The bound on $p_{\rm ann}$ includes annihilation channels into all visible SM final states (i.e., excluding neutrino final states). In our case, the final states are dominantly electrons (and muons for DM masses above the muon mass), and we include the relevant branching fractions as appropriate when computing the total annihilation cross section. In the case of multiple possible final states, we weight the cross sections by the relevant deposited energy efficiency fraction, $f_{\rm eff}$. Since the DM particles are highly nonrelativistic during and after recombination, to obtain $\langle \sigma v \rangle_{\rm CMB}$ we evaluate Eq. (6) in the limit $\epsilon \to 0$,

$$\langle \sigma v \rangle_{\rm CMB} = \frac{\alpha g_\chi^2 \kappa^2}{s_0^2} \frac{(s_0 + 2m_e^2)\sqrt{(s_0 - 4m_e^2)(s_0 - \delta^2)}}{B_e(\sqrt{s_0})((1+\epsilon_R)\Gamma_{A'}^2 + s_0 \epsilon_R^2)}. \tag{19}$$

To compute the CMB limit on our parameter space, we require that the total $f_{\rm eff}$-weighted cross section in Eq. (19) not exceed the one implied by the bound on $p_{\rm ann}$. The excluded parameters are depicted in Fig. 2 as dotted lines

which, despite being excluded by the CMB, would yield the observed amount of DM, as described in the previous section. We find that—in contrast to the case of nonresonant pseudo-Dirac DM—very small mass splittings and large excited state fractions remain unconstrained by the CMB, particularly in the part of the plane corresponding to small couplings. Additionally, for the sub-keV values of δ that we consider here, the bound from the CMB is independent of δ because we do not get a substantial enough suppression in the excited state abundance as a result of the early kinetic decoupling (i.e., $f^* \sim 1$ near the boundary of the CMB exclusion).

C. Self-interacting DM

Models of inelastic DM can also have unique SIDM behavior in DM halos, affecting density profiles and subhalo mass functions in a way that is distinct from purely elastic SIDM [62,63]. In this model, elastic scattering between the ground and excited states can occur at tree level, which is especially relevant in the thermal histories we consider where it is possible to have a high abundance of the excited state at late times. As we are in the Born regime, $\alpha_\chi m_\chi / m_{A'} \approx \alpha_\chi / 2 \ll 1$, we can use results previously derived in the literature for the relevant SIDM cross sections. The s-channel resonance is not typically relevant in astrophysical environments (in contrast to, e.g., Ref. [64]), since the lowest value of ϵ_R we consider is $\sim 10^{-3}$ due to the strong BBN constraints described in Sec. III A, which corresponds to a minimum resonant velocity of $\sim 10^4$ km/s, in contrast to the $\sim 10^2$ km/s velocities that are typical in galaxies like the Milky Way.

For tree-level elastic scattering between the ground and excited states, we employ the Born cross section of Ref. [65], assuming that the t-channel dominates. We find that the elastic scattering cross section is generally much less than the $\sigma/m_\chi \sim 1\ \mathrm{cm}^2/\mathrm{g}$ characteristic of SIDM constraints from merging galaxy clusters [66]. The exception to this lies at the edge of perturbativity $g_\chi \sim 1$ for the lightest DM masses we consider, $m_\chi \sim 10$ MeV. However, this part of the parameter space is excluded by the CMB, as is evident from Fig. 2. Even if the CMB constraint could be circumvented, in this part of the parameter space the abundance of excited state particles (which would be required for tree-level elastic scattering) is generally more suppressed as shown in Fig. 4, which would also weaken the bounds from merging clusters. Elastic scattering between particles in the same mass state (i.e., two ground state particles) only occurs at the one-loop level in this model; we confirm that the cross sections for these processes fall well below the $\sim 1\ \mathrm{cm}^2/\mathrm{g}$ level (due to the α_χ^4 scaling) using the expressions in the Supplemental Materials of Ref. [57]. We therefore conclude that merging cluster constraints on elastic SIDM do not have any impact in the viable parameter space for this model.

Upscattering from the ground state to the excited state is kinematically forbidden below the velocity threshold of $v \sim \sqrt{\delta/m_\chi}$, which can take on a wide range of values in the parameter space we consider, some of which are relevant to astrophysical systems. Above this velocity threshold, the cross section for upward scattering in the Born regime saturates to the value of the elastic cross section between the ground and excited states [67]; while this cross section is generally below $\sim 1\ \mathrm{cm}^2/\mathrm{g}$ in our parameter space, the endothermic nature of the scattering can lead to substantial qualitative differences in the DM distribution compared to the elastic scattering case [63], and therefore strong conclusions cannot be drawn about observational prospects without dedicated simulation work. Similarly, downward scattering from the excited state to the ground state takes on the same value as upward scattering once the velocities are above threshold; below threshold, there is an enhancement to the downscattering cross section, rendering it potentially quite large at low velocities (with $\sigma/m_\chi \gg 1\ \mathrm{cm}^2/\mathrm{g}$). The effects of inelastic scattering have only begun to be explored in simulation, with no direct analog of this situation having been analyzed. In this thermal history, up to 50% of the DM begins in the excited state similar to Ref. [62], which showed that even a few percent of the DM downscattering can have a significant effect on the structure of DM halos. On the other hand, the velocity thresholds in our parameter space can be easily accessible in astrophysical systems, potentially leading to some upward scattering, which has a highly nontrivial interplay with the effects of downscattering as studied in Ref. [63]. Clearly further exploration of the parameter space in simulation will be fruitful for connecting late-Universe halo observables to DM parameters motivated by self-consistent DM thermal histories.

D. Indirect detection

DM annihilation in astrophysical environments produces cosmic rays and high-energy photons, which can be employed to search indirectly for DM. A null detection of annihilation byproducts can thus be used to constrain the annihilation cross section, $\langle \sigma v \rangle$. The strength of the expected signal additionally depends on the integrated DM density (the J factor). As discussed in the previous subsection, SIDM effects, particularly those from inelastic interactions, may alter the expected density profiles of DM halos. As this has yet to be quantified via simulation, we assume in this discussion that resonant inelastic DM has the same J factor as what is typically considered in the literature. Additionally, as shown in Sec. III, the CMB constraints on DM annihilation push us toward $g_\chi \lesssim 0.1$, which corresponds to the ground and excited states being equally populated, or $f^* \sim 1$, for the δ ranges of interest (see also Fig. 4). Therefore, as opposed to standard thermal histories of inelastic DM, we do not necessarily have a late-time

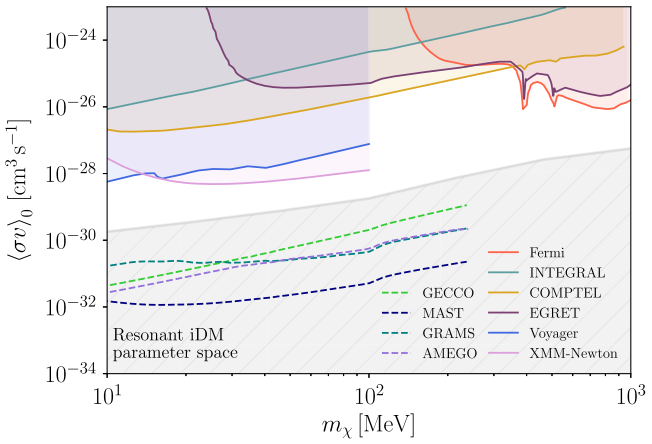

FIG. 5. Bounds on the total DM annihilation cross section as a function of DM mass from various γ-ray and x-ray experiments [61,68,69] (solid lines) as well as projections [70–76] (dashed lines). The resonant inelastic DM parameter space allowed by the CMB is shown in gray.

suppression of annihilation from the thermal depletion of the excited state.

Since the DM velocity in present-day halos is too small (by about 2 orders of magnitude) for the dark photon mediator to be produced on shell, the DM annihilation rate at late times can be calculated in the heavy mediator (nonresonant) limit. In Fig. 5, we show the constraints on the *total* present-day DM annihilation cross section to SM states, $\langle\sigma v\rangle_0$, from measurements of the gamma-ray flux from the Galactic Center using Fermi INTEGRAL, COMPTEL, and EGRET [61]. We also show constraints from Voyager [68] and XMM-Newton [69], which bound the DM annihilation cross section to electrons and therefore have been cut off at the muon threshold, $m_\mu \sim 100$ MeV beyond which annihilation to other final states becomes relevant. For reference, we show the resonant pseudo-Dirac DM parameter region allowed by the CMB in gray. Even though current constraints do not yet probe the target parameter space that is allowed by the CMB, future telescopes such as GECCO [70,71], MAST [72], GRAMS [73,74], and AMEGO [75,76] will be able to explore the parameter space [77].

IV. TERRESTRIAL SEARCHES

A. Accelerator searches

Accelerator experiments provide a complementary probe to search for DM and any associated mediators. Dark photons with masses in the MeV–GeV range can be produced at collider and beam dump experiments, resulting in either missing transverse energy or displaced vertex signatures. The production cross section for the dark photons depends on their coupling to the SM, κ, whereas the decay signature depends on their lifetime, $\tau_{A'} = 1/\Gamma_{A'}$ which is in general a function of $\kappa, g_\chi, \epsilon_R$, and δ. Since $\delta \ll m_{A'}, m_\chi$, one can assume to a very good approximation that $\Gamma_{A'}$ is independent of δ (i.e., we can take $\delta \to 0$). In this limit, the bounds presented in Ref. [45] which were obtained using a modified version of DarkCast [78] can be directly applied to our parameter space. In particular, as was pointed out in Ref. [45], for a given $m_{A'}$, the constraints on κ depend only on a combination of g_χ and ϵ_R through the dark photon's reduced invisible decay width,

$$\gamma_{\rm inv} \equiv \frac{\Gamma_{A'}}{m_{A'}} = \frac{g_\chi^2}{12}\left(1-\frac{1}{1+\epsilon_R}\right)^{1/2}\left(1+\frac{1}{2(1+\epsilon_R)}\right). \quad (20)$$

In Fig. 6, we display the bounds on dark photons in the κ-$m_{A'}$ plane for two fixed values of the dark photon's reduced invisible width, $\gamma_{\rm inv} = 10^{-5}$ (left) and $\gamma_{\rm inv} = 10^{-13}$ (right). The shaded regions correspond to different dark photon production channels. For $\gamma_{\rm inv} = 10^{-5}$, the invisible decay width is larger than the visible one for $\kappa \lesssim 0.1$, and therefore the beam dump experiments that search for A' decays to leptons lose sensitivity. The solid black lines in both panels correspond to the κ values that reproduce the observed DM abundance following the production mechanism outlined in Sec. II, for $\epsilon_R \in [0.001, 0.1]$. The dashed parts of the black lines correspond to the points excluded by the CMB. We note that for $\Gamma_{\rm DM} > \Gamma_{\rm SM}$, (or equivalently $g_\chi \gg \kappa$), the CMB constrains the part of the parameter space which cannot be probed by accelerator experiments making the accelerator and cosmological bounds highly complementary. Additionally, we find that for a given $\gamma_{\rm inv}$ and ϵ_R, or equivalently, a fixed g_χ, there exists a maximum $m_{A'}$ beyond which DM is always overproduced. From Eq. (14), we see that the DM relic density is proportional to $m_{A'}/\min(g_\chi^2, \kappa^2)$ meaning that once the couplings are fixed, a larger $m_{A'}$ results in a larger DM abundance. This causes the relic lines to be vertical in the right panel of Fig. 6 (in the left panel, the maximum $m_{A'}$ lies outside the plotted region). Finally, we note that for a given $\gamma_{\rm inv}$, κ values bounded by the two curves corresponding to $\epsilon_R = 0.001$ and $\epsilon_R = 0.1$ also reproduce the observed DM abundance for different values of ϵ_R resulting in a much broader thermal target. For reference, we show the usual thermal target assuming nonresonant, s-wave thermal freeze-out (dotted black line) in the left panel of Fig. 6. Future accelerator experiments are poised to more fully explore the parameter space of this model, as shown in Fig. 7.

B. Direct detection

Most thermal histories for pseudo-Dirac DM result in a relic excited state fraction suppressed by several orders of magnitude such that most of the DM in the halo of the Milky Way (MW) is in the ground state. In this case, because of the off diagonal coupling, the only tree-level scattering process on a SM target would be upward scattering to the excited state. In contrast, for the thermal

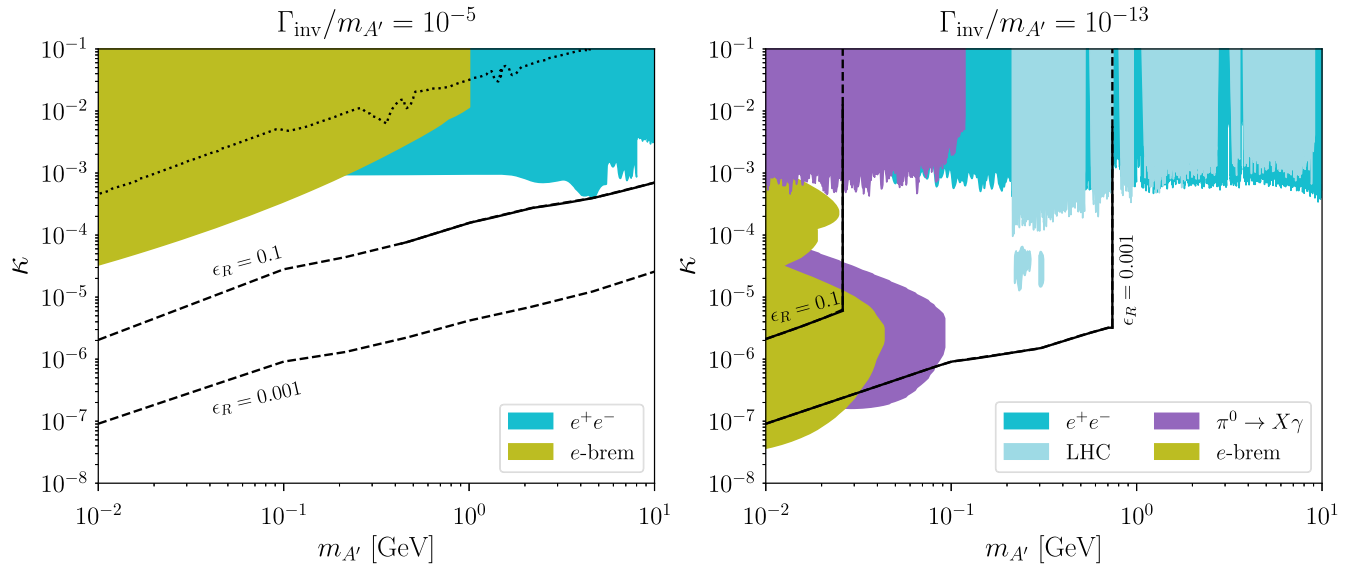

FIG. 6. Some of the strongest constraints in the κ-$m_{A'}$ plane from accelerator experiments, including *BABAR* [79–81], NA64 [82,83], LHCb [84,85], CMS [86], NuCal [87,88], E141 [89], NA48 [90], and E137 [91], as computed with DarkCast [78]. The different colors correspond to different dark photon production channels. We show two representative cases where the dark photon decays primarily invisibly (left) and visibly (right). The solid black lines represent the target for $\epsilon_R = 0.001$ and $\epsilon_R = 0.1$, with the dashed portions corresponding to exclusions from the CMB. Also shown for comparison is the thermal prediction assuming thermal freeze-out with $m_{A'} = 3m_\chi$ (dotted line) [48].

history considered in this work, around half of the DM is in the excited state at late times for most parts of the parameter space. In particular, the largest values of g_χ that suppress the abundance of χ_2 in this thermal history are already excluded by the CMB (see Figs. 2 and 4). Therefore, the primary signature of pseudo-Dirac DM in direct detection experiments is downscattering of the excited state $\chi_2 e \to \chi_1 e$, which deposits an energy $\sim\delta$. The deposited energy can ionize electrons in the target which can be detected either directly through charge-coupled devices [102], or by detecting secondary scintillation photons using photomultiplier tubes [103]. The absence of a kinematic

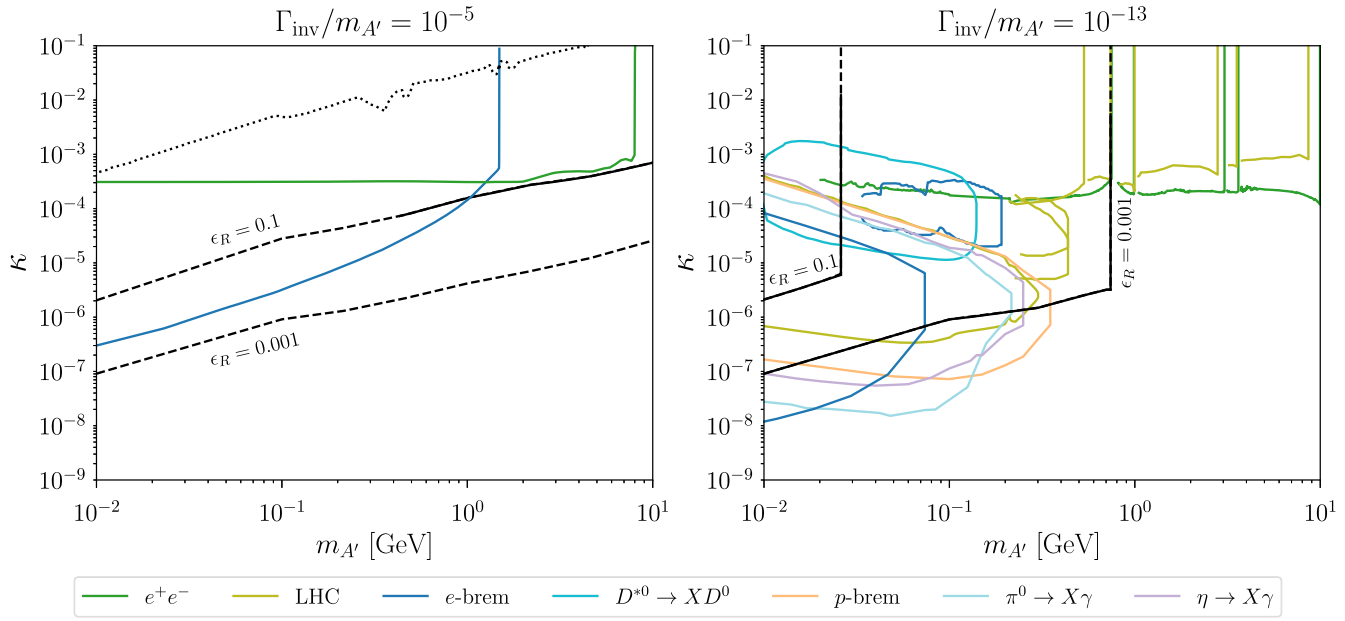

FIG. 7. Same as Fig. 6 except with some of the strongest projections for future experiments including Belle II [92], FASER [93], HPS [94], LDMX [95], LHCb [96,97], SeaQuest [98], SHiP [99,100], and Yemilab [101].

barrier for downscattering implies an enhancement in the event rate for sub-GeV DM.

In the following discussion, we consider DM-electron scattering in semiconductor and Xenon targets, and we place constraints on the fiducial DM-electron scattering cross section [20],

$$\bar{\sigma}_e = \frac{4\mu_{\chi,e}^2 \alpha \kappa^2 g_\chi^2}{(m_{A'}^2 + \alpha^2 m_e^2)^2}, \tag{21}$$

where $\mu_{\chi,e}$ is the reduced mass of the DM-electron system. The recoil energy of the electron is $E_{\rm Re} = \Delta E_e - \Delta E_B$ where ΔE_B is the electron binding energy and the energy deposited by sub-GeV DM downscattering is

$$\Delta E_e = \mathbf{q}\cdot\mathbf{v} - \frac{\mathbf{q}^2}{2m_\chi} + \delta \tag{22}$$

for momentum transfer $\mathbf{q}$ and relative velocity $\mathbf{v}$. For downscattering, the minimum velocity required to transfer a momentum with magnitude q and an energy ΔE_e to the electron is therefore given by

$$v_{\rm min}(q, \Delta E_e) \equiv \left| \frac{\Delta E_e - \delta}{q} + \frac{q}{2m_\chi} \right|, \tag{23}$$

which corresponds to the differential event rate for atomic targets [20,104],

$$\frac{{\rm d}R}{{\rm d}\Delta E_e} = \frac{\bar{\sigma}_e}{8\mu_{\chi e}^2} \sum_{n,l} (\Delta E_e - E_{nl})^{-1} \frac{\rho_{\chi_2}}{m_{\chi_2}} \times \int q{\rm d}q |f_{nl\to\Delta E_e - E_{nl}}(q)|^2 \eta(v_{\rm min}(q, \Delta E_e)), \tag{24}$$

where $\Delta E_{n,l}$ is the binding energy of the electron in the nl shell, $\rho_{\chi_2} = f^* \rho_{\rm DM} \approx 0.5 \times 0.4\ {\rm GeV\,cm^{-3}}$ is the density of the excited state [51], and $f_{nl\to\Delta E_e - E_{nl}}(q)$ is the electron ionization form factor which we evaluated numerically following the prescription of Ref. [105] using DarkART [106]. The function $\eta(v_{\rm min})$ in Eq. (24) can be related to the DM-velocity distribution $f_\chi(v)$ by

$$\eta(v_{\rm min}) \equiv \int \frac{d^3 v}{v} f_\chi(v) \Theta(v - v_{\rm min}). \tag{25}$$

In this work, we assume the Standard Halo Model for $f_\chi(v)$ [107]. The magnitude of the momentum transferred to the electron for a given DM mass and energy deposition ΔE_e is bounded by

$$q_{\rm min} = {\rm sign}(\Delta E_e - \delta) m_\chi v_{\rm max} \left(1 - \sqrt{1 - \frac{\Delta E_e - \delta}{\frac{1}{2} m_\chi v_{\rm max}^2}}\right)$$
$$q_{\rm max} = m_\chi v_{\rm max} \left(1 + \sqrt{1 - \frac{\Delta E_e - \delta}{\frac{1}{2} m_\chi v_{\rm max}^2}}\right), \tag{26}$$

where $v_{\rm max}$ is the largest DM velocity relative to the detector frame as determined by the escape velocity of the halo at the Earth's position and the velocity of Earth in the Galactic rest frame [107]. A similar expression as Eq. (24) can be obtained for semiconductor targets which depends instead on the crystal form factor as described in Ref. [21]. The relevant energy threshold for such a target is the band gap between the valence band and the conduction band. Note that in Eq. (24), we have set the DM form factor to unity, $F_{\rm DM} = 1$, which corresponds to the heavy mediator limit, $m_{A'} \gg \alpha m_e$ as determined by the typical Fermi momentum (for semiconductor targets) or inverse Bohr radius (for atomic targets).

In contrast to the case of elastic scattering, the minimum momentum transfer, $q_{\rm min}$ for a given energy transfer ΔE_e, can be zero if the mass splitting is above the energy threshold for ionization. This results in much larger event rates since the inelastic scattering kinematics have substantial overlap with peaks in the electron ionization form factor [108]. A similar effect also occurs for semiconductor targets where the peaks in the crystal form factor become more kinematically accessible for $\delta > 0$ [21]. Inelastic scattering also results in a characteristic spectrum of events peaked around $\Delta E_e \sim \delta$. As a result, bounds on $\bar{\sigma}_e$ derived under the assumption of elastic scattering cannot be directly applied to the parameter space of this model.

In order to recast the bounds, we use the prescription outlined in Ref. [109] for calculating event rates in the XENON10 [109,110], XENON1T [103], and SENSEI [111] experiments. For XENON10 and XENON1T, we calculate the electron ionization form factors using DarkART [106]. The crystal form factors for SENSEI are obtained from QEDark [21]. We use the publicly available data for the three experiments [103,109–111] to derive 90% confidence level exclusions on $\bar{\sigma}_e$, shown in Fig. 8. For XENON10 and XENON1T, we show the exclusion for $\delta = 10$ eV and $\delta = 100$ eV, while for SENSEI, we show the exclusion for $\delta = 10$ eV. We verify that our analysis reproduces the elastic scattering ($\delta = 0$) bounds from these experiments, shown as shaded regions in Fig. 8. We note that these bounds are conservative since we do not model any backgrounds or place any cuts in the observed events. In other words, we treat any event as a potential DM signal, resulting in the weakest possible limits on the cross section.

As shown in Fig. 8, the allowed parameter space of this model (represented by the gray band) is an attractive target for upcoming experiments probing light DM. In particular, we plot the sensitivity curves for Oscura [112] for $\delta = 0$ eV (light purple) and $\delta = 10$ eV (purple) assuming an exposure

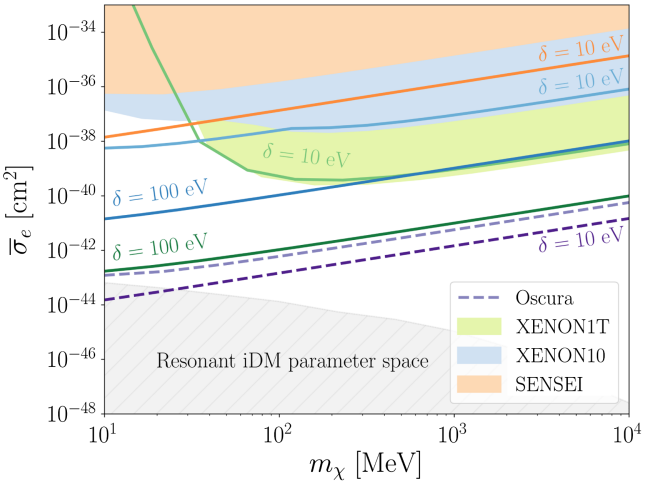

FIG. 8. Constraints on the DM-electron scattering cross section, σ_e as a function of the DM mass from XENON10 (blue), XENON1T (green), and SENSEI (orange) for different values of δ, with $f^* = 1$. The shaded regions correspond to exclusions on elastic scattering, i.e., $\delta = 0$. The dashed purple lines are sensitivity curves for Oscura assuming $\delta = 0$ (light) and $\delta =$ 10 eV (dark) respectively. In gray, we show the resonant inelastic DM parameter space allowed by CMB.

of 30 kg-year. Furthermore, for the $\mathcal{O}$(eV) values of δ we consider here, upward scattering inside the Earth may result in an enhanced density of the excited state at the detector, which would also result in stronger bounds and forecasts than the ones presented here [108]. Finally, even stronger bounds and forecasts may be obtained by considering electron ionization caused by DM-nucleon scattering through the Migdal effect [113–115]. These bounds were evaluated for $\delta \gtrsim O(\text{keV})$ in Ref. [116]. We leave an analysis of these bounds for sub-keV values of δ for future work.

V. DISCUSSION

Pseudo-Dirac DM is a minimal modification of standard vector portal DM that can result in qualitatively new cosmological, astrophysical, and experimental phenomenology. In this work, we examine the parameter space of this well-studied model in the regime of small (sub-keV) mass splittings and in the presence of resonant annihilations, $\chi_2\chi_1 \to A' \to \text{SM SM}$, where $m_{A'} \approx 2m_\chi$. The resonantly enhanced annihilations imply that tiny couplings are able to reproduce the observed DM relic density. Additionally, because of these small couplings, DM can kinetically decouple from the SM before its final relic abundance is reached. Therefore, in order to accurately predict the relic density, one must solve a coupled system of Boltzmann equations for the densities and temperatures of the relevant species. We used the numerical Boltzmann solver DRAKE to properly account for this effect and found that the predicted DM abundance can have corrections as large as an order of magnitude, depending on the underlying parameters of the theory.

The early kinetic decoupling ensures that the excited state is not thermally depleted. Despite the presence of the excited state, this model is consistent with strong bounds coming from BBN and the CMB owing to the strong velocity suppression in the annihilation cross section at sub-keV temperatures (when the dark photon can no longer be produced on shell). As a result, as shown in Fig. 2, most of the parameter space of this model is unconstrained, in contrast to sub-GeV Dirac DM that freezes out through an s-wave process.

The presence of the long-lived excited state can have unique astrophysical signatures that are usually not relevant for pseudo-Dirac DM. For instance, tree-level elastic scattering could cause SIDM behavior, with the caveat that cross sections exceeding $\sigma/m_\chi \sim 1$ cm^2/g either have couplings that are excluded by the CMB or lie in a region of parameter space with $f^* \sim 0.01$. More notably, exothermic downward scattering can be relevant, especially in low-velocity environments where there is an enhancement to the cross section. The extent to which exothermic scattering matters *in situ* is difficult to quantify without further simulation of inelastic SIDM halos; however previous work has found that small mass splittings with $\delta/m_\chi \sim 10^{-6}$ can have a dramatic impact on the properties of a DM halo and its subhalos [62,63]. The relic excited state can also result in signals in indirect detection experiments. The ground and excited state present in the MW can annihilate into various SM states, and therefore gamma-ray and x-ray telescopes can be used to look for signatures of this model. Since DM annihilation at late times mimics the off resonance Dirac case, we use previous analyses of gamma-ray and x-ray data [61,68,69] to place bounds on the total DM annihilation cross section. We find that despite the small couplings, the resonant inelastic parameter space is an attractive target for the next generation of telescopes such as GECCO, MAST, GRAMS, and AMEGO (see Fig. 5).

The excited state can downscatter in a range of direct detection experiments. Because of the absence of a kinematic barrier for this process, the event rate is significantly enhanced compared to elastic scattering and also compared to pseudo-Dirac DM thermal histories with an exponentially suppressed abundance of the excited state. Using state-of-the-art numerical codes DarkART and QEDark to obtain the electron ionization and crystal form factors respectively, we calculate the event rates for inelastic DM-electron scattering at Xenon- and Silicon-based experiments. We use the analysis procedure described in Ref. [109] to place bounds on the DM-electron scattering cross section for different values of δ. We find that future semiconductor-based experiments such as Oscura will begin to probe the resonant inelastic DM parameter space as shown in Fig. 8.

Simultaneously, accelerator searches for dark photons can also explore relevant parameter space for this model. We use the publicly available code DarkCast, to depict bounds on the kinetic mixing, κ for fixed values of g_χ. The presence of a resonance implies a broadening of the thermal target as shown in Fig. 6. We find that accelerator bounds are complementary to those set by the CMB, as the accelerator experiments probe the parts of the parameter space that are harder to constrain using early-Universe probes. Future experiments will constrain large parts of the parameter space of this model, as shown in Fig. 7.

In summary, sub-GeV resonant pseudo-Dirac DM is an attractive thermal target for a variety of terrestrial DM experiments and astrophysical searches. The complete exploration of the phenomenology of this model leaves a lot of promising directions for future work. In particular, a more accurate treatment of the photodisassociation bounds coming from BBN may further constrain this parameter space. Additionally, the early kinetic decoupling present in this model may loosen the $m_\chi \geq 10$ MeV lower bound on the mass of thermal DM coming from $N_{\rm eff}$, despite the thermal equilibrium between the dark and visible sectors at early times. Furthermore, it will be necessary to perform additional cosmological simulations in order to understand the effect of upward and downward scattering on halo properties which have immediate consequences for direct and indirect detection experiments. Finally, a more rigorous analysis of the direct detection bounds needs to be undertaken, including (1) the upward scattering of the ground state as it passes through the Earth before downward scattering in the detector and (2) scattering on electrons through the Migdal effect. Such an analysis may result in even stronger bounds and forecasts on resonant pseudo-Dirac DM than the ones presented here.

ACKNOWLEDGMENTS

It is a pleasure to thank Daniel Baxter, Asher Berlin, Elias Bernreuther, Timon Emken, Felix Kahlhoefer, Tongyan Lin, and Tien-Tien Yu for useful conversations and correspondence pertaining to this work. We especially thank Neal Weiner for useful comments on the manuscript. The research of N. B. was undertaken thanks in part to funding from the Canada First Research Excellence Fund through the Arthur B. McDonald Canadian Astroparticle Physics Research Institute. S. H. was supported in part by a Trottier Space Institute Fellowship. N. B., S. H., and K. S. acknowledge support from a Natural Sciences and Engineering Research Council of Canada Subatomic Physics Discovery Grant and from the Canada Research Chairs program.

[1] Gerard Jungman, Marc Kamionkowski, and Kim Griest, Supersymmetric dark matter, Phys. Rep. **267**, 195 (1996).
[2] Benjamin W Lee and Steven Weinberg, Cosmological lower bound on heavy-neutrino masses, Phys. Rev. Lett. **39**, 165 (1977).
[3] Keith R. Dienes, Christopher F. Kolda, and John March-Russell, Kinetic mixing and the supersymmetric gauge hierarchy, Nucl. Phys. **B492**, 104 (1997).
[4] Bob Holdom, Two U(1)'s and epsilon charge shifts, Phys. Lett. **166B**, 196 (1986).
[5] S. A. Abel and B. W. Schofield, Brane anti-brane kinetic mixing, millicharged particles and SUSY breaking, Nucl. Phys. **B685**, 150 (2004).
[6] S. Abel and Jose Santiago, Constraining the string scale: From Planck to weak and back again, J. Phys. G **30**, R83 (2004).
[7] S. A. Abel, M. D. Goodsell, J. Jaeckel, V. V. Khoze, and A. Ringwald, Kinetic mixing of the photon with hidden U(1)s in string phenomenology, J. High Energy Phys. 07 (2008) 124.
[8] Bobby S. Acharya, Sebastian A. R. Ellis, Gordon L. Kane, Brent D. Nelson, and Malcolm J. Perry, The lightest visible-sector supersymmetric particle is likely to be unstable, Phys. Rev. Lett. **117**, 181802 (2016).
[9] Bobby S. Acharya, Sebastian A. R. Ellis, Gordon L. Kane, Brent D. Nelson, and Malcolm Perry, Categorisation and detection of dark matter candidates from string/M-theory hidden sectors, J. High Energy Phys. 09 (2018) 130.
[10] G. Aldazabal, Luis E. Ibanez, F. Quevedo, and A. M. Uranga, D-branes at singularities: A bottom up approach to the string embedding of the standard model, J. High Energy Phys. 08 (2000) 002.
[11] Brian Batell and Tony Gherghetta, Localized U(1) gauge fields, millicharged particles, and holography, Phys. Rev. D **73**, 045016 (2006).
[12] Tony Gherghetta, Jörn Kersten, Keith Olive, and Maxim Pospelov, Evaluating the price of tiny kinetic mixing, Phys. Rev. D **100**, 095001 (2019).
[13] Giorgio Arcadi, Maíra Dutra, Pradipta Ghosh, Manfred Lindner, Yann Mambrini, Mathias Pierre, Stefano Profumo, and Farinaldo S. Queiroz, The waning of the WIMP? A review of models, searches, and constraints, Eur. Phys. J. C **78**, 203 (2018).
[14] Jennifer M. Gaskins, A review of indirect searches for particle dark matter, Contemp. Phys. **57**, 496 (2016).
[15] C. Boehm and Pierre Fayet, Scalar dark matter candidates, Nucl. Phys. **B683**, 219 (2004).
[16] Maxim Pospelov, Adam Ritz, and Mikhail B. Voloshin, Secluded WIMP dark matter, Phys. Lett. B **662**, 53 (2008).
[17] Jonathan L. Feng and Jason Kumar, The WIMPless miracle: Dark-matter particles without weak-scale masses or weak interactions, Phys. Rev. Lett. **101**, 231301 (2008).

[18] Yonit Hochberg, Eric Kuflik, Hitoshi Murayama, Tomer Volansky, and Jay G. Wacker, Model for thermal relic dark matter of strongly interacting massive particles, Phys. Rev. Lett. **115**, 021301 (2015).
[19] Gordan Krnjaic, Probing light thermal dark-matter with a Higgs portal mediator, Phys. Rev. D **94**, 073009 (2016).
[20] Rouven Essig, Jeremy Mardon, and Tomer Volansky, Direct detection of Sub-GeV dark matter, Phys. Rev. D **85**, 076007 (2012).
[21] Rouven Essig, Marivi Fernandez-Serra, Jeremy Mardon, Adrian Soto, Tomer Volansky, and Tien-Tien Yu, Direct detection of sub-GeV dark matter with semiconductor targets, J. High Energy Phys. 05 (2016) 046.
[22] R. Agnese *et al.* (SuperCDMS Collaboration), First dark matter constraints from a SuperCDMS single-charge sensitive detector, Phys. Rev. Lett. **121**, 051301 (2018); **122**, 069901(E) (2019).
[23] P. Agnes *et al.* (DarkSide Collaboration), Constraints on Sub-GeV dark-matter–electron scattering from the DarkSide-50 experiment, Phys. Rev. Lett. **121**, 111303 (2018).
[24] A. Aguilar-Arevalo *et al.* (DAMIC Collaboration), Constraints on light dark matter particles interacting with electrons from DAMIC at SNOLAB, Phys. Rev. Lett. **123**, 181802 (2019).
[25] Q. Arnaud *et al.* (EDELWEISS Collaboration), First germanium-based constraints on sub-MeV dark matter with the EDELWEISS experiment, Phys. Rev. Lett. **125**, 141301 (2020).
[26] Yonatan Kahn and Tongyan Lin, Searches for light dark matter using condensed matter systems, Rep. Prog. Phys. **85**, 066901 (2022).
[27] Tracy R. Slatyer, Indirect dark matter signatures in the cosmic dark ages. I. Generalizing the bound on s-wave dark matter annihilation from Planck results, Phys. Rev. D **93**, 023527 (2016).
[28] N. Aghanim *et al.* (Planck Collaboration), Planck 2018 results. VI. Cosmological parameters, Astron. Astrophys. **641**, A6 (2020); **652**, C4(E) (2021).
[29] David Tucker-Smith and Neal Weiner, Inelastic dark matter, Phys. Rev. D **64**, 043502 (2001).
[30] Douglas P. Finkbeiner and Neal Weiner, Exciting dark matter and the INTEGRAL/SPI 511 keV signal, Phys. Rev. D **76**, 083519 (2007).
[31] Nima Arkani-Hamed, Douglas P. Finkbeiner, Tracy R. Slatyer, and Neal Weiner, A theory of dark matter, Phys. Rev. D **79**, 015014 (2009).
[32] Clifford Cheung, Joshua T. Ruderman, Lian-Tao Wang, and Itay Yavin, Kinetic mixing as the origin of light dark scales, Phys. Rev. D **80**, 035008 (2009).
[33] Fang Chen, James M. Cline, and Andrew R. Frey, Non-Abelian dark matter: Models and constraints, Phys. Rev. D **80**, 083516 (2009).
[34] Brian Batell, Maxim Pospelov, and Adam Ritz, Direct detection of multi-component secluded WIMPs, Phys. Rev. D **79**, 115019 (2009).
[35] Peter W. Graham, Roni Harnik, Surjeet Rajendran, and Prashant Saraswat, Exothermic dark matter, Phys. Rev. D **82**, 063512 (2010).
[36] Gilly Elor, Hongwan Liu, Tracy R. Slatyer, and Yotam Soreq, Complementarity for dark sector bound states, Phys. Rev. D **98**, 036015 (2018).
[37] Michael Duerr, Torben Ferber, Camilo Garcia-Cely, Christopher Hearty, and Kai Schmidt-Hoberg, Long-lived dark Higgs and inelastic dark matter at Belle II, J. High Energy Phys. 04 (2021) 146.
[38] Michael Duerr, Torben Ferber, Christopher Hearty, Felix Kahlhoefer, Kai Schmidt-Hoberg, and Patrick Tunney, Invisible and displaced dark matter signatures at Belle II, J. High Energy Phys. 02 (2020) 039.
[39] Haipeng An, P. S. Bhupal Dev, Yi Cai, and R. N. Mohapatra, Sneutrino dark matter in gauged inverse see-saw models for neutrinos, Phys. Rev. Lett. **108**, 081806 (2012).
[40] Douglas P. Finkbeiner and Neal Weiner, X-ray line from exciting dark matter, Phys. Rev. D **94**, 083002 (2016).
[41] Mariana Carrillo González and Natalia Toro, Cosmology and signals of light pseudo-Dirac dark matter, J. High Energy Phys. 04 (2022) 060.
[42] Masha Baryakhtar, Asher Berlin, Hongwan Liu, and Neal Weiner, Electromagnetic signals of inelastic dark matter scattering, J. High Energy Phys. 06 (2022) 047.
[43] Kim Griest and David Seckel, Three exceptions in the calculation of relic abundances, Phys. Rev. D **43**, 3191 (1991).
[44] Paolo Gondolo and Graciela Gelmini, Cosmic abundances of stable particles: Improved analysis, Nucl. Phys. **B360**, 145 (1991).
[45] Elias Bernreuther, Saniya Heeba, and Felix Kahlhoefer, Resonant sub-GeV dirac dark matter, J. Cosmol. Astropart. Phys. 03 (2021) 040.
[46] Eder Izaguirre, Gordan Krnjaic, Philip Schuster, and Natalia Toro, Analyzing the discovery potential for light dark matter, Phys. Rev. Lett. **115**, 251301 (2015).
[47] Jonathan L. Feng and Jordan Smolinsky, Impact of a resonance on thermal targets for invisible dark photon searches, Phys. Rev. D **96**, 095022 (2017).
[48] Asher Berlin, Nikita Blinov, Gordan Krnjaic, Philip Schuster, and Natalia Toro, Dark matter, millicharges, axion and scalar particles, gauge bosons, and other new physics with LDMX, Phys. Rev. D **99**, 075001 (2019).
[49] Saniya Heeba, Tongyan Lin, and Katelin Schutz, Inelastic freeze-in, Phys. Rev. D **108**, 095016 (2023).
[50] V. V. Ezhela, S. B. Lugovsky, and O. V. Zenin, Hadronic part of the muon g-2 estimated on the sigma**2003(tot) (e+e-—> hadrons) evaluated data compilation, arXiv:hep-ph/0312114.
[51] M. Tanabashi *et al.* (Particle Data Group), Review of particle physics, Phys. Rev. D **98**, 030001 (2018).
[52] Laura G. van den Aarssen, Torsten Bringmann, and Yasar C. Goedecke, Thermal decoupling and the smallest sub-halo mass in dark matter models with Sommerfeld-enhanced annihilation rates, Phys. Rev. D **85**, 123512 (2012).
[53] Tobias Binder, Torsten Bringmann, Michael Gustafsson, and Andrzej Hryczuk, Early kinetic decoupling of dark matter: When the standard way of calculating the thermal relic density fails, Phys. Rev. D **96**, 115010 (2017); **101**, 099901(E) (2020).

[54] Tobias Binder, Torsten Bringmann, Michael Gustafsson, and Andrzej Hryczuk, Dark matter relic abundance beyond kinetic equilibrium, Eur. Phys. J. C **81**, 577 (2021).
[55] Tobias Binder, Torsten Bringmann, Michael Gustafsson, and Andrzej Hryczuk, Dark matter relic density revisited: The case for early kinetic decoupling, in *Proceedings of the 53rd Rencontres de Moriond on Electroweak Interactions and Unified Theories* (2018), pp. 245–250, arXiv:1805.00526.
[56] Tobias Binder, Torsten Bringmann, Michael Gustafsson, and Andrzej Hryczuk, Early kinetic decoupling of dark matter: When the standard way of calculating the thermal relic density fails, Phys. Rev. D **96**, 115010 (2017).
[57] Patrick J. Fitzpatrick, Hongwan Liu, Tracy R. Slatyer, and Yu-Dai Tsai, New thermal relic targets for inelastic vector-portal dark matter, Phys. Rev. D **106**, 083507 (2022).
[58] Paul Frederik Depta, Marco Hufnagel, Kai Schmidt-Hoberg, and Sebastian Wild, BBN constraints on the annihilation of MeV-scale dark matter, J. Cosmol. Astropart. Phys. 04 (2019) 029.
[59] Nashwan Sabti, James Alvey, Miguel Escudero, Malcolm Fairbairn, and Diego Blas, Refined bounds on MeV-scale thermal dark sectors from BBN and the CMB, J. Cosmol. Astropart. Phys. 01 (2020) 004.
[60] Marco Cirelli, Gennaro Corcella, Andi Hektor, Gert Hutsi, Mario Kadastik, Paolo Panci, Martti Raidal, Filippo Sala, and Alessandro Strumia, PPPC 4 DM ID: A poor particle physicist cookbook for dark matter indirect detection, J. Cosmol. Astropart. Phys. 03 (2011) 051; 10 (2012) E01.
[61] Adam Coogan, Logan Morrison, Tilman Plehn, Stefano Profumo, and Peter Reimitz, Hazma meets HERWIG4DM: Precision gamma-ray, neutrino, and positron spectra for light dark matter, J. Cosmol. Astropart. Phys. 11 (2022) 033.
[62] Mark Vogelsberger, Jesús Zavala, Katelin Schutz, and Tracy R. Slatyer, Evaporating the Milky Way halo and its satellites with inelastic self-interacting dark matter, Mon. Not. R. Astron. Soc. **484**, 5437 (2019).
[63] Stephanie O'Neil *et al.*, Endothermic self-interacting dark matter in Milky Way-like dark matter haloes, Mon. Not. R. Astron. Soc. **524**, 288 (2023).
[64] Xiaoyong Chu, Camilo Garcia-Cely, and Hitoshi Murayama, Velocity dependence from resonant self-interacting dark matter, Phys. Rev. Lett. **122**, 071103 (2019).
[65] Jonathan L. Feng, Manoj Kaplinghat, and Hai-Bo Yu, Halo shape and relic density exclusions of Sommerfeld-enhanced dark matter explanations of cosmic ray excesses, Phys. Rev. Lett. **104**, 151301 (2010).
[66] Sean Tulin and Hai-Bo Yu, Dark matter self-interactions and small scale structure, Phys. Rep. **730**, 1 (2018).
[67] Katelin Schutz and Tracy R. Slatyer, Self-scattering for dark matter with an excited state, J. Cosmol. Astropart. Phys. 01 (2015) 021.
[68] Mathieu Boudaud, Julien Lavalle, and Pierre Salati, Novel cosmic-ray electron and positron constraints on MeV dark matter particles, Phys. Rev. Lett. **119**, 021103 (2017).
[69] Marco Cirelli, Nicolao Fornengo, Jordan Koechler, Elena Pinetti, and Brandon M. Roach, Putting all the X in one basket: Updated x-ray constraints on sub-GeV dark matter, J. Cosmol. Astropart. Phys. 07 (2023) 026.
[70] Elena Orlando *et al.*, Exploring the MeV sky with a combined coded mask and Compton telescope: The galactic explorer with a coded aperture mask Compton telescope (GECCO), J. Cosmol. Astropart. Phys. 07 (2022) 036.
[71] Adam Coogan *et al.*, Hunting for dark matter and new physics with GECCO, Phys. Rev. D **107**, 023022 (2023).
[72] Timur Dzhatdoev and Egor Podlesnyi, Massive argon space telescope (MAST): A concept of heavy time projection chamber for γ-ray astronomy in the 100 MeV–1 TeV energy range, Astropart. Phys. **112**, 1 (2019).
[73] Tsuguo Aramaki, Per Hansson Adrian, Georgia Karagiorgi, and Hirokazu Odaka, Dual MeV gamma-ray and dark matter observatory—GRAMS project, Astropart. Phys. **114**, 107 (2020).
[74] Tsuguo Aramaki *et al.*, Snowmass 2021 letter of interest: The GRAMS project: MeV gamma-ray observations and antimatter-based dark matter searches, arXiv:2009.03754.
[75] Regina Caputo *et al.* (AMEGO Collaboration), All-sky medium energy gamma-ray observatory: Exploring the extreme multimessenger universe, arXiv:1907.07558.
[76] Carolyn A. Kierans (AMEGO Team), AMEGO: Exploring the extreme multimessenger universe, Proc. SPIE Int. Soc. Opt. Eng. **11444**, 1144431 (2020).
[77] Adam Coogan, Logan Morrison, and Stefano Profumo, Precision gamma-ray constraints for sub-GeV dark matter models, J. Cosmol. Astropart. Phys. 08 (2021) 044.
[78] Philip Ilten, Yotam Soreq, Mike Williams, and Wei Xue, Serendipity in dark photon searches, J. High Energy Phys. 06 (2018) 004.
[79] J. P. Lees *et al.* (*BABAR* Collaboration), Search for invisible decays of a dark photon produced in e^+e^- collisions at *BABAR*, Phys. Rev. Lett. **119**, 131804 (2017).
[80] J. P. Lees *et al.* (*BABAR* Collaboration), Search for a dark photon in e^+e^- collisions at *BABAR*, Phys. Rev. Lett. **113**, 201801 (2014).
[81] J. P. Lees *et al.* (*BABAR* Collaboration), Search for a muonic dark force at *BABAR*, Phys. Rev. D **94**, 011102 (2016).
[82] D. Banerjee *et al.*, Dark matter search in missing energy events with NA64, Phys. Rev. Lett. **123**, 121801 (2019).
[83] D. Banerjee *et al.*, Improved limits on a hypothetical X (16.7) boson and a dark photon decaying into e^+e^- pairs, Phys. Rev. D **101**, 071101 (2020).
[84] Roel Aaij *et al.* (LHCb Collaboration), Search for dark photons produced in 13 TeV pp collisions, Phys. Rev. Lett. **120**, 061801 (2018).
[85] Roel Aaij *et al.* (LHCb Collaboration), Search for $A' \to \mu^+\mu^-$ decays, Phys. Rev. Lett. **124**, 041801 (2020).
[86] CMS Collaboration, Search for a narrow resonance lighter than 200 GeV Decaying to a pair of muons in proton-proton collisions at $\sqrt{s} = 13$ TeV, Phys. Rev. Lett. **124**, 131802 (2020).
[87] Yu-Dai Tsai, Patrick deNiverville, and Ming Xiong Liu, The high-energy frontier of the intensity frontier: Closing the dark photon, inelastic dark matter, and Muon g-2 windows, Phys. Rev. Lett. **126**, 181801 (2021).
[88] J. Blumlein *et al.*, Limits on neutral light scalar and pseudoscalar particles in a proton beam dump experiment, Z. Phys. C **51**, 341 (1991).

[89] E. M. Riordan *et al.*, A search for short lived axions in an electron beam dump experiment, Phys. Rev. Lett. **59**, 755 (1987).
[90] J. R. Batley *et al.* (NA48/2 Collaboration), Search for the dark photon in π^0 decays, Phys. Lett. B **746**, 178 (2015).
[91] Sarah Andreas, Carsten Niebuhr, and Andreas Ringwald, New limits on hidden photons from past electron beam dumps, Phys. Rev. D **86**, 095019 (2012).
[92] E. Kou *et al.*, The Belle II Physics Book, Prog. Theor. Exp. Phys. **2019**, 123C01 (2019).
[93] Akitaka Ariga *et al.* (FASER Collaboration), FASER's physics reach for long-lived particles, Phys. Rev. D **99**, 095011 (2019).
[94] N. Baltzell *et al.* (HPS Collaboration), The heavy photon search beamline and its performance, Nucl. Instrum. Methods Phys. Res., Sect. A **859**, 69 (2017).
[95] Torsten Åkesson *et al.* (LDMX Collaboration), Light dark matter experiment (LDMX), arXiv:1808.05219.
[96] Philip Ilten, Jesse Thaler, Mike Williams, and Wei Xue, Dark photons from charm mesons at LHCb, Phys. Rev. D **92**, 115017 (2015).
[97] Philip Ilten, Yotam Soreq, Jesse Thaler, Mike Williams, and Wei Xue, Proposed inclusive dark photon search at LHCb, Phys. Rev. Lett. **116**, 251803 (2016).
[98] S. Gardner, R. J. Holt, and A. S. Tadepalli, New prospects in fixed target searches for dark forces with the SeaQuest experiment at Fermilab, Phys. Rev. D **93**, 115015 (2016).
[99] Sergey Alekhin *et al.*, A facility to search for hidden particles at the CERN SPS: The SHiP physics case, Rep. Prog. Phys. **79**, 124201 (2016).
[100] C. Ahdida *et al.* (SHiP Collaboration), Sensitivity of the SHiP experiment to dark photons decaying to a pair of charged particles, Eur. Phys. J. C **81**, 451 (2021).
[101] Seon-Hee Seo and Yeongduk Kim, Dark photon search at Yemilab, Korea, J. High Energy Phys. 04 (2021) 135.
[102] Liron Barak *et al.* (SENSEI Collaboration), SENSEI: Characterization of single-electron events using a skipper charge-coupled device, Phys. Rev. Appl. **17**, 014022 (2022).
[103] E. Aprile *et al.* (XENON Collaboration), Light dark matter search with ionization signals in XENON1T, Phys. Rev. Lett. **123**, 251801 (2019).
[104] Itay M. Bloch, Andrea Caputo, Rouven Essig, Diego Redigolo, Mukul Sholapurkar, and Tomer Volansky, Exploring new physics with O(keV) electron recoils in direct detection experiments, J. High Energy Phys. 01 (2021) 178.
[105] Riccardo Catena, Timon Emken, Nicola A. Spaldin, and Walter Tarantino, Atomic responses to general dark matter-electron interactions, Phys. Rev. Res. **2**, 033195 (2020).
[106] Timon Emken, Dark Atomic Response Tabulator (DarkART)[Code, v0.1.0], The code can be found under https://github.com/temken/darkart (2021).
[107] N. Wyn Evans, Ciaran A. J. O'Hare, and Christopher McCabe, Refinement of the standard halo model for dark matter searches in light of the Gaia Sausage, Phys. Rev. D **99**, 023012 (2019).
[108] Timon Emken, Jonas Frerick, Saniya Heeba, and Felix Kahlhoefer, Electron recoils from terrestrial upscattering of inelastic dark matter, Phys. Rev. D **105**, 055023 (2022).
[109] Rouven Essig, Tomer Volansky, and Tien-Tien Yu, New constraints and prospects for sub-GeV dark matter scattering off electrons in XENON, Phys. Rev. D **96**, 043017 (2017).
[110] J. Angle *et al.* (XENON10 Collaboration), A search for light dark matter in XENON10 data, Phys. Rev. Lett. **107**, 051301 (2011); **110**, 249901(E) (2013).
[111] Liron Barak *et al.* (SENSEI Collaboration), SENSEI: Direct-detection results on sub-GeV dark matter from a new skipper-CCD, Phys. Rev. Lett. **125**, 171802 (2020).
[112] Alexis Aguilar-Arevalo *et al.* (Oscura Collaboration), The Oscura experiment, arXiv:2202.10518.
[113] Masahiro Ibe, Wakutaka Nakano, Yutaro Shoji, and Kazumine Suzuki, Migdal effect in dark matter direct detection experiments, J. High Energy Phys. 03 (2018) 194.
[114] E. Aprile *et al.* (XENON Collaboration), Search for light dark matter interactions enhanced by the Migdal effect or bremsstrahlung in XENON1T, Phys. Rev. Lett. **123**, 241803 (2019).
[115] A. Migdal, J. Phys. (USSR) **4**, 449 (1941).
[116] Nicole F. Bell, James B. Dent, Bhaskar Dutta, Sumit Ghosh, Jason Kumar, and Jayden L. Newstead, Low-mass inelastic dark matter direct detection via the Migdal effect, Phys. Rev. D **104**, 076013 (2021).